# Probing variations of fibrous structures during the development of breast ductal carcinoma tissues via Mueller matrix imaging

**YANG DONG,**[1,6] **SHAOXIONG LIU,**[2,6,7] **YUANXING SHEN,**[3,4] **HONGHUI HE,**[3,*] [ID] **AND HUI MA**[1,3,5,8]

[1]*Center for Precision Medicine and Healthcare, Tsinghua-Berkeley Shenzhen Institute, Tsinghua University, Shenzhen 518071, China*
[2]*Shenzhen Sixth People's Hospital (Nanshan Hospital) Huazhong University of Science and Technology Union Shenzhen Hospital, Shenzhen 518052, China*
[3]*Guangdong Research Center of Polarization Imaging and Measurement Engineering Technology, Shenzhen Key Laboratory for Minimal Invasive Medical Technologies, Institute of Optical Imaging and Sensing, Tsinghua Shenzhen International Graduate School, Tsinghua University, Shenzhen 518055, China*
[4]*Department of Biomedical Engineering, Tsinghua University, Beijing 100084, China*
[5]*Department of Physics, Tsinghua University, Beijing 100084, China*
[6]*These authors contributed equally to this work*
[7]*liusx20088@sina.com*
[8]*mahui@tsinghua.edu.cn*
[*]*he.honghui@sz.tsinghua.edu.cn*

**Abstract:** Recently, we developed a label-free method to probe the microstructural information and optical properties of unstained thin tissue slices based on microscopic Mueller matrix imaging technique. In this paper, we take the microscopic Mueller matrix images of human breast ductal carcinoma tissue samples at different pathological stages, and then calculate and analyze their retardance-related Mueller matrix-derived parameters. To reveal the microstructural features more quantitatively and precisely, we propose a new method based on first-order statistical properties of image to transform the 2D images of Mueller matrix parameters into several statistical feature vectors. We evaluate each statistical feature vector by corresponding classification characteristic value extracted from the statistical features of Mueller matrix parameters images of healthy breast duct tissue samples. The experimental results indicate that these statistical feature vectors of Mueller matrix derived parameters may become powerful tools to quantitatively characterize breast ductal carcinoma tissue samples at different pathological stages. It has the potential to facilitate automating the staging process of breast ductal carcinoma tissue, resulting in the improvement of diagnostic efficiency.

## 1. Introduction

Breast cancer incidence has been increasing for decades worldwide, and this megatrend will carry on into the future with tremendous damage and suffering to the physical and mental health of women [1,2]. According to the most recent data on cancer incidence, mortality, and survival in women compiled by the American Cancer Society in 2019, breast cancer accounts for 30% of all estimated new cancer diagnoses and 15% of all estimated cancer deaths [3,4]. Breast cancer is heterogeneous: more than 20 distinct histopathological subtypes have been identified, which are clinically relevant with tumor grade and stage, classification according to estrogen receptor $\alpha$ and progesterone receptor status, assessment by immunohistochemistry (IHC), and so on [5,6]. Breast ductal carcinoma is a common type of breast cancer starts in cells that line the mammary ducts, which carry breast milk to the nipple. Clinically, there are two types of breast ductal carcinoma due to different expression of gene and epigenome: ductal carcinoma *in situ* (DCIS) and invasive

ductal carcinoma (IDC) [7,8]. Generally, DCIS is an early stage of breast ductal carcinoma in which epithelial cells with similar features of infiltrating carcinoma have proliferated within mammary ducts but have not yet invaded surrounding tissues, while IDC refers to a later stage of breast ductal carcinoma that carcinoma cells have broken through the wall of the mammary ducts and begun to invade the tissues of the breast, and even spread to the lymph nodes and other areas of body [9,10]. It has been testified that young women with benign lesion of fibrocystic change and breast ductal carcinoma are highly susceptible to develop advanced malignant lesions as age increasing [11]. Clearly early diagnosis is a vital step in the treatment of breast ductal carcinoma. The gold standard of cancer diagnosis currently is the microscopic examination of histological tissue slices that are stained with certain dyes such as hematoxylin and eosin (H and E) to reveal qualitative morphological information on pathological samples [12,13]. The limits of conventional histological analysis are that the diagnosis accuracy relies heavily on the clinical experience and pathological knowledge of pathologists, and the staining process of histological sections may destroy the tissue samples' microstructures, then complicates the diagnosis process and prolongs the diagnosis time. Recently, for quantitative evaluation of breast ductal carcinoma tissues, more and more optical methods have been developed, such as the second harmonic generation (SHG) technique [14], the Mueller matrix imaging technique [15], and so on.

Experimental evidence has demonstrated that both the structure and composition of collagenous components of breast ductal tissues undergo alterations with tumor initiation and progression [16]. Mueller matrix imaging, as a type of polarimetry, has many unique advantages as a promising label-free technique for detecting tissue microstructures, especially the anisotropic fibrous components in complex biological specimens [17–19], including breast ductal carcinoma tissues. As a comprehensive characterization of the polarization properties of the sample, Mueller matrix can reveal abundant structural information and optical properties of tissues and other scattering media. Hence it has found applications in various biomedical studies and practices [17–21], as well as the characterization of textiles [22] and polymers [23]. Recently, we have reported a modulus-designed Mueller matrix microscope by adding both the polarization states generator and analyzer (PSG and PSA) to a commercial transmission-light optical microscope. It provides a powerful tool for obtaining the wavelength-scale microstructural information of tissues [24]. Preliminary biomedical applications on pathological tissue samples, such as liver fibrosis [25], gastrointestinal luminal tuberculosis [26] and breast ductal carcinoma [15,27,28], have shown the diagnostic potential of such Mueller matrix microscope and Mueller matrix derived parameters.

Previously, we used the Mueller matrix microscope and retardance-related Mueller matrix derived parameters as the detection and staging tools of human breast ductal carcinoma tissues at different progression stages [15]. However, for clinical diagnosis a detailed comparison among different parameters is crucial, and more quantitative indicators are needed. Here in this study, we propose a new method to obtain a set of statistical feature vectors of the Mueller matrix parameters by dividing the original parameter images into blocks and deriving the statistical characteristics of each image block. We also compare the statistical characteristics of the potentially useful Mueller matrix parameters between normal and abnormal breast ductal tissue samples. The results indicate that these statistical feature vectors of Mueller matrix derived parameters may become powerful tools to quantitatively and objectively characterize breast ductal carcinoma tissue samples at different pathological stages. Compared to the conventional histological analysis for breast ductal tissue samples, the proposed technique in this study is capable of probing more microstructural information and optical properties of unstained pathological tissue sections, deriving quantitative indicators for objective evaluation, and potentially facilitating the training procedure of pathologists. Therefore, it has the potential to facilitate automating the staging process of breast ductal carcinoma tissue, resulting in the improvement of diagnostic efficiency.

## 2. Materials and methods

### 2.1. Experimental setup

Here we use the transmission Mueller matrix microscope upgraded from a commercial optical microscope (L2050, Liss Optical Instrument Factory, Guangzhou, China) by adding the compact polarization states generator (PSG) and analyzer (PSA) modules based on the dual rotating retarder method [29,30]. As shown in Fig. 1, the illuminating light from the light-emitting diode (632 nm, 3 W, Cree, China) passes through the PSG module where the polarization states of incident light can be controlled by a polarizer with the horizontal polarization direction (P1, extinction ratio 500:1, Daheng Optics, China) and a rotatable quarter-wave plate (R1, Daheng Optics, China). The light beams with different polarization states transmit the sample on the stage and the objective lens. It is then analyzed by the PSA module consisting of another rotatable quarter-wave plate (R2, Daheng Optics, China) and polarizer with the horizontal polarization direction (P2, extinction ratio 500:1, Daheng Optics, China), and recorded by a 12-bit CCD camera (QImaging 74-0107A, Canada).
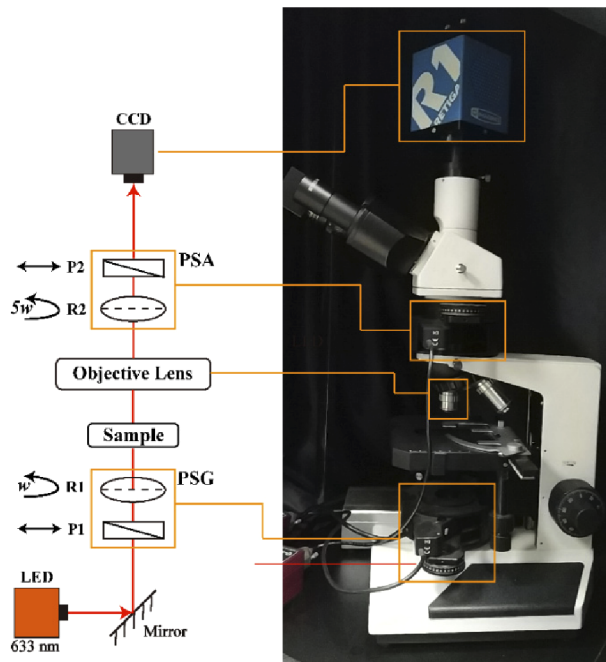


**Fig. 1.** Photograph and schematic of the Mueller matrix microscope. P: polarizer; R: quarter-wave plate; PSG: polarization states generator; PSA: polarization states analyzer.

In each measurement, the two retarders (R1, R2) rotate thirty times in total with a fixed rate of $\omega_2=5\omega_1$. After obtaining 30 images with specific polarization input and output states, the Mueller matrix elements can be calculated by using the Fourier coefficients [31]. Before applying to the tissue samples, the microscope was calibrated and compensated by measuring the Mueller matrices of standard samples such as air, polarizers and retarders. As shown in Eq. (1), $M_{sample}$ represents the true Mueller matrix of the sample, $M_{objective}^{-1}$ represents the compensating matrix of the microscope system, $M_{measured}$ represents the measured Mueller matrix of the sample in the experiment. Comparing the mean values of each element of standard samples' Mueller matrix before and after the calibration, we can see that the maximum error of the Mueller matrix microscope has been reduced to 0.01. More details about the calibration process and result of the

microscope can be found in [30].

$$M_{sample} = M_{objective}^{-1} \times M_{measured} \tag{1}$$

### 2.2. Mueller matrix polar decomposition and transformation parameters

Mueller matrix contains abundant polarization-related structural information of a scattering sample. For explicit analysis of Mueller matrix, some methods to transform Mueller matrix elements into parameters with clearer physical and structural meanings have been proposed. In this work, we adopt the linear retardation-related Mueller matrix polar decomposition (MMPD) and Mueller matrix transformation (MMT) parameters, which were used in our previous studies on breast ductal carcinoma tissue samples [15]. The MMPD method proposed by Lu and Chipman decomposes a Mueller matrix into three sub-matrices reflecting three main physical properties of a medium: diattenuation ($D$), retardance ($R$), and depolarization ($\Delta$) [32]. Accordingly, a series of orientation-insensitive parameters have been extracted from the MMPD method and applied to the detections of various cancerous tissues [33,34]. In this study, we used the linear retardance ($\delta$) shown as Eq. (2) to describe the fibrous structures in breast ductal carcinoma tissue samples.

$$M = M_\Delta M_R M_D$$
$$\delta = \cos^{-1}\left\{ [(M_R(2,2) + M_R(3,3))^2 + (M_R(3,2) + M_R(2,3))^2]^{\frac{1}{2}} - 1 \right\} \tag{2}$$

Where $\delta$ is derived from $M_R$ which is the sub-matrix of retardance decomposed from Mueller matrix ($M$) [35].

Besides, we also proposed the MMT technique to obtain a set of polarization parameters which are functions of different Mueller matrix elements and have clear associations with the microstructures of samples [19,36]. Equation (3) defines the parameter $t$ used in this study.

$$t = \frac{\sqrt{(m42)^2 + (m43)^2}}{2} \tag{3}$$

It has been demonstrated from experiments and simulations that the MMPD parameter $\delta$ and MMT parameter $t$ can be used to reveal the density and alignment orderness of the fibrous structures [25,37]. Besides, the retardance-related information is mainly reflected in the Mueller matrix elements m24, m34, m42 and m43. As shown in Eq. (3), the parameter $t$ is linearly correlated with the root-mean-square of the m42 and m43, which is one of the rotation invariant parameters representing the capability of transforming between linear and circular polarizations [38]. However, the individual Mueller matrix elements with positive and negative values often lack of explicit connections to the characteristic microstructures of tissues and the measurement can be affected by the orientations of anisotropic structures. Here in this study the proposed method is more effective for the analysis of Mueller matrix parameters with positive values. Therefore, we also take the absolute value of Mueller matrix element $|m43|$ as a comparative group to verify the ability of the individual Mueller matrix element combined with proposed method to stage breast ductal carcinoma tissues. Of note, the absolute values of Mueller matrix elements $|m24|$, $|m34|$ and $|m42|$ can also be used for the comparative study. The Mueller matrix elements are all normalized by m11, therefore, the values of Mueller matrix parameters $|m43|$ and $t$ range from 0 to 1. For the parameter $\delta$, its physical unit is radian which ranges from 0 to $\pi$, whereas, in the transmission Mueller matrix measurement of thin breast duct tissue sections, the values of linear retardance parameter $\delta$ are relatively small distributing in the range of 0-0.15. Therefore, in the following section of methodology, the frequency distribution statistics of Mueller matrix parameters $|m43|$, $t$ and $\delta$ are all carried out in the range of 0-1.

## 2.3.   Breast duct tissue sample

We choose some unstained, dewaxed pathological sections of breast ductal carcinoma tissue slices at different stages as the samples for the Mueller matrix microscope as Figs. 2(a2) - 2(e2). The samples are all 12-μm-thick slices prepared and provided by Shenzhen Sixth People's (Nanshan) Hospital. In addition to the tissue slices in stage 1 (normal), stage 2 (ductal carcinoma *in situ*) and stage 3 (invasive ductal carcinoma), we also acquire the samples between normal and ductal carcinoma *in situ* grouped as stage 1_2, and those between ductal carcinoma *in situ* and invasive ductal carcinoma grouped as stage 2_3. The 12-μm-thick breast ductal tissues were cut from the dehydrated paraffins for preparing unstained pathological sections, and for histological comparison, the corresponding 4-μm-thick tissues were cut from the same positions for preparing hematoxylin and eosin (H and E) stained slices, which are supposed to have the same pathological structural features. However, it seems that there are some differences between the microscopic images of the two kinds of pathological slides from Fig. 2, because of (1) the thickness difference between the two pathological slides and (2) there are some deformations and damages for microstructures of the corresponding 4-μm-thick tissues for preparing H&E stained slices during the dyeing process.
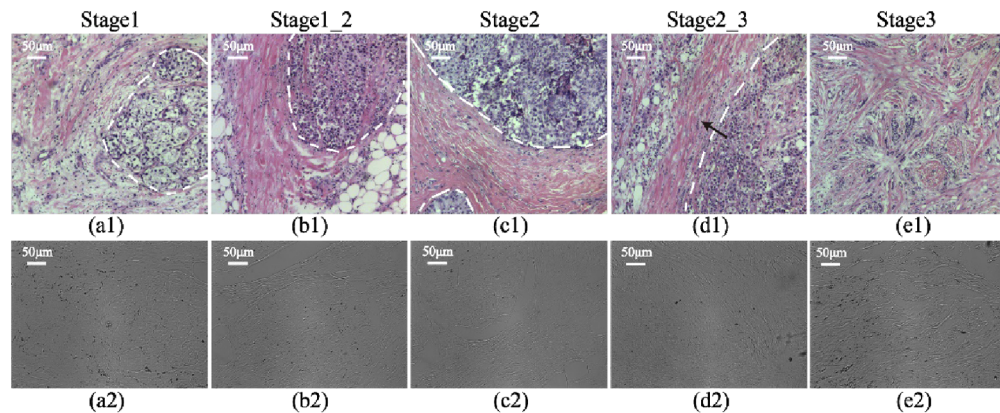


**Fig. 2.** Microscopic images of the H and E stained slices of breast ductal tissues at different pathological stages: (a1) stage 1; (b1) stage 1_2; (c1) stage 2; (d1) stage 2_3; (e1) stage 3, and the corresponding 12-μm-thick unstained dewaxed slices of breast ductal tissues: (a2) stage 1; (b2) stage 1_2; (c2) stage 2; (d2) stage 2_3; (e2) stage 3.

As shown in Figs. 2(a1)–2(e1), the qualitative observations of H and E images indicate that the fibrous structures in and around the breast catheters (the boundaries marked by the white dotted lines) have different proportions and distributions for breast ductal carcinoma tissues at different pathological stages. Specifically, there is no obvious proliferation of collagen fibers (pink under H and E staining) in normal breast tissues, as shown in Fig. 2(a1). During the process of carcinogenesis, the abnormal cell nuclei (indigo blue under H and E staining) inside the catheter and the fibers outside the catheter proliferate gradually and obviously. The alignment orientation directions of the fibers are shown to be roughly circular aligned in the peripheral regions surrounding the ducts, as shown in Figs. 2(b1)–2(c1). In Fig. 2(d1), we can observe that the malignant cells begin to break through the basement membrane of the breast duct (along the direction marked by the arrow) and spread out to invade the surrounding tissues. With the development and infiltration of the tumor cells, there is no obvious duct boundary in stage 3 shown as Fig. 2(e1). The densely and orderly distributed fibers around breast catheter are destroyed completely, and hyperplastic collagen fibers fill the whole breast ductal carcinoma tissue. Meanwhile we can observe that from the un-polarized intensity images of unstained

breast histological slices shown as Figs. 2(a2)–2(e2), the fibrous structures in breast ductal tissues can hardly be discriminated. However, the 2D images of Mueller matrix parameters of these samples shown in the following sections clearly display fibrous structures, which pave the way for quantitative evaluation of fibers' proportion variations in breast ductal carcinoma at different stages. In this work, 50 breast ductal tissue samples at different stages (10 samples for each stage) were analyzed. This work was approved by the Ethics Committee of the Shenzhen Sixth People's (Nanshan) Hospital.

### 2.4. Statistical feature vectors of Mueller matrix parameters images

In our previous studies, we found that the 2D images of Mueller matrix elements or derived parameters can be transformed into frequency distribution histogram (FDH) curves and central moment parameters by statistical analysis [21,22,39]. The idea of exploiting the spatial features of polarimetric images has been explored by several other groups in recent years [40–42]. As the first-order statistical properties of image, FDHs can be used as tools for analyzing but have limited potential in describing detailed image texture features. In order to take advantage of the local structural information of image to quantitatively characterize microstructural differences among breast ductal carcinoma samples at different stages, here we explore the method of statistical feature vectors of Mueller matrix parameters images. To illustrate, the Mueller matrix element $|m43|$, MMT parameter $t$ and MMPD parameter $\delta$ images of 990×1260 pixels are all divided into 55×60 pixels patches in sequence. Therefore, as shown in Fig. 3(a), 378 image blocks can be obtained from each image. Six statistical characteristic parameters-$m$, $std$, $R$, $u_3$, $U$ and $e$-of each image block based on FDHs can be calculated, and there are 378 sets of statistical characteristic parameters can be obtained from each Mueller matrix parameter image. More details about how to calculate six statistical characteristic parameters of polarimetric image blocks can be found in the Supplement 1 Section "*Six statistical characteristic parameters of polarimetric image blocks*". Here, the expected value $m$ is the mean value, and $std$ is the standard deviation of all pixel values in this image. $R$ is supposed to be a measurement of relative smoothness of image texture brightness. Smoothness value ranges from 0 to 1, and for regions with identical pixel values, the value of $R$ is 1. Similarly, $U$ represents the consistency of the image. When the pixel values of the image are the same, $U$ has the maximum value of 1. The fourth statistical characteristic parameter $u3$ is called skewness, which can be positive or negative. A positive (or negative) skewness value represents that the tail on the right side (or the left side) of the FDHs is longer or fatter than the left side (or the right side). The last statistical characteristic parameter $e$, known as entropy, has the potential to measure randomness of the image. The larger value of entropy means greater uncertainty and randomness of the image.

As shown in Fig. 3(b), along the direction indicated by the red arrow, the six statistical characteristic parameters calculated from each image block are added to the corresponding statistical feature vectors in sequence, and finally six statistical feature vectors with 378 components ($\overline{m}$, $\overline{std}$, $\overline{R}$, $\overline{u3}$, $\overline{U}$ and $\overline{e}$) are formed. Therefore, with six statistical feature vectors in a Mueller matrix parameter image, we can digitize 2D information of microstructures of human breast ductal carcinoma tissues.

### 2.5. Scoring parameters derived from statistical feature vectors of Mueller matrix parameters

To obtain more quantitative information on the microstructures of breast ductal carcinoma tissues from the Mueller matrix parameters images, here we adopt a new method based on statistical feature vectors for the experimental data of all the samples automatically and quantitatively. Firstly, we calculate the mean value of 378 components in each statistical feature vector for Mueller matrix parameters of the normal samples in stage 1, and the total mean values of six statistical feature vectors-$f\_m$, $f\_std$, $f\_R$, $f\_u3$, $f\_U$ and $f\_e$-for 10 normal samples are used as
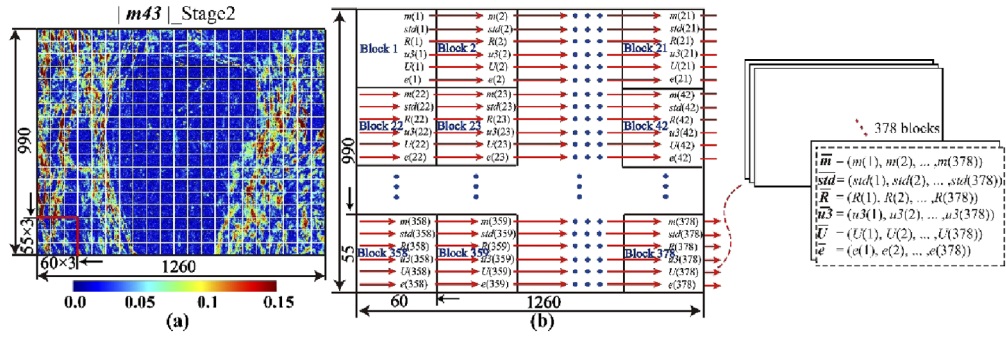
**Fig. 3.** Process of 2D polarization image digitization: (a) Pseudo-color image of Mueller matrix parameter |*m43*| of a 12-μm-thick unstained dewaxed slice of breast ductal carcinoma *in situ*. Different blocks are marked by white squares; (b) Diagram of the method for getting six statistical feature vectors from a polarimetric image.

a criterion denoted as classification characteristic values, to distinguish polarimetric images between normal and carcinoma samples. The Section "*Six classification characteristic values obtained from normal breast ductal tissue samples*" in Supplement 1 provides the details about how to calculate the six classification characteristic values from normal breast tissues. In order to evaluate the microstructures of breast ductal carcinoma tissues during the process of initiation and development progress more quantitatively and objectively, then we propose a scoring parameter shown as Eq. (4), in which $N_{above}$ and $N_{below}$ represent the numbers of components that are above and below the classification characteristic value respectively in each statistical feature vector. *N_parameters* is a general term for the values calculated from statistical feature vectors $\overline{m}, \overline{std}, \overline{R}, \overline{u3}, \overline{U}$ and $\overline{e}$ according to Eq. (4), and can be denoted as *N_m, N_std, N_R, N_u3, N_U* and *N_e* respectively.

$$N\_parameters = \frac{N_{above}}{N_{below}} \tag{4}$$

### 2.6. Evaluation parameters for characterization ability of different Mueller matrix parameters

For quantitative comparisons of differentiation ability of different Mueller matrix parameters for breast ductal carcinoma samples using statistical feature vectors, a parameter, named *r_values*, is defined as Eq. (5) according to the definition of overlapping coefficient [43], indicating the overlapping ratio of *N_parameters* in two adjacent stages during the development of breast ductal carcinoma. The overlapping coefficient is defined as a measure of the agreement between two probability distributions. Mathematically, it can be calculated from the overlapping area of two probability distribution curves [43]. Since the size of data to be evaluated is relatively small here, we chose the ratio of the two data sets' overlapping data range to overall range as a measure of their agreement or similarity. The range of the parameter *r_values* is from 0 (separating two adjacent stages completely) to 1 (overlapping two adjacent stages completely). Therefore, a smaller value of *r_values* means a more prominent differentiation ability of the corresponding *N_parameters*. In Eq. (5), $x_{max}$ and $x_{min}$ represent the maximum and minimum of *N_parameters* in the previous stage respectively, and $y_{max}$ and $y_{min}$ are the corresponding values of later stage in

the two adjacent stages.

$$r\_values = \begin{cases} \frac{x_{max}-y_{min}}{y_{max}-x_{min}} & (N\_parameters = N\_m, N\_std, N\_u3, N\_e) \\ \\ \frac{y_{max}-x_{min}}{x_{max}-y_{min}} & (N\_parameters = N\_R, N\_U) \end{cases} \tag{5}$$

## 3. Results and discussion

### 3.1. Microscopic imaging results of breast duct tissue samples

The microscopic images of the $|m43|$, MMT parameter $t$ and MMPD parameter $\delta$ of the breast duct tissue samples at different pathological stages are shown in Fig. 4, with boundaries of the breast catheters marked by the white dotted lines. We can see that the image contrasts of parameter $t$ and $\delta$ are similar, and are better than that of $|m43|$. The fibrous structures in and around ducts characterized by the three polarimetric parameters have the following distribution and proportion variations at different stages: (1) compared with the normal tissues (stage 1) shown as Fig. 4(a), the parameters' values of the fibrous structural components surrounding the lumen in stage 1_2 shown as Fig. 4(b) are obviously higher than those inside the ducts, which means the retardance around the ducts in the tissues increases gradually with the occurrence of ductal carcinoma, while that in the internal regions of the ducts remains almost the same; (2) when the abnormal tissues develop into ductal carcinoma *in situ* (stage 2) shown as Fig. 4(c), the fibrous structures around the ducts are much more prominent with dramatically increased parameters' values compared with those in stage 1_2; (3) unlike the dense and aligned fibrotic areas immediately surrounding the ducts in stage 2, the basement membrane of the duct is destructed and broken down gradually during the process of infiltration and metastasis of carcinoma cells accompanied by fibroplasias in stage 2_3. It can be observed clearly from Fig. 4(d) that, in contrast to Fig. 4(c), there is a slight reduction of the parameters' values surrounding the catheter and an observable increase inside the catheter, indicating fibers exist both within and without the ducts at this stage; (4) for invasive ductal carcinoma tissues in stage 3 presented as Fig. 4(e), high retardance structures are quite prominent not just in the areas surrounding ducts but also within the ducts themselves. It can be concluded from Fig. 4(e) and our previous study that the proportion of fibrous structures, which can be quantitatively evaluated by the Mueller matrix parameters, is notable both inside and outside the ducts with a more disordered distribution behavior [15]. The main reasons leading to the characteristic variations of retardance-related Mueller matrix-derived parameters' values within and without the ducts in breast ductal tissues at different pathological stages include: (1) extracellular matrix (ECM), i.e. the micro-environmental conditions that cells find themselves in, will be remodeling during the breast tumor progression. It has been reported that ECM remodeling plays a critical role in the control and regulation of tumorigenesis and metastatic progression of breast ductal carcinoma [44]. At the time of carcinogenesis, a transformation event results in cells invasion into the breast lumen. After that, the abnormal cells multiply within the breast catheter, and the ECM remodeling increases the linearity and density of collagen fibers dramatically surrounding the catheter, resulting in primary breast ducal carcinoma where the basement membrane attached to the basal surface of breast duct epithelial cells is intact [45], i.e. breast ductal carcinoma *in situ*. In addition, experiments and simulations in our previous studies have shown that the retardance-related Mueller matrix-derived parameters are good and quantitative indicators of fibrous structures [25,38]. Therefore, an increasing of retardance surrounding the breast catheter is observed for breast ductal carcinoma *in situ* with respect to the normal breast ductal tissue; (2) the increased linearity and density of collagen fibers in pre-malignant tissue were shown to contribute to malignant transformation in the breast tissues [46]. The lysyl oxidase (LOX) secreted by hypoxic carcinoma cells inside the breast duct increases invasion, destroying the basement membrane and enabling metastatic dissemination.

There is no obvious duct boundary in invasive breast ductal carcinoma, and malignant cells together with proliferative fibers fill the entire breast tissue [47]. Therefore, an increasing of the retardance is observed both within and without the breast ducts for invasive breast ductal carcinoma compared to the normal breast ductal tissue.
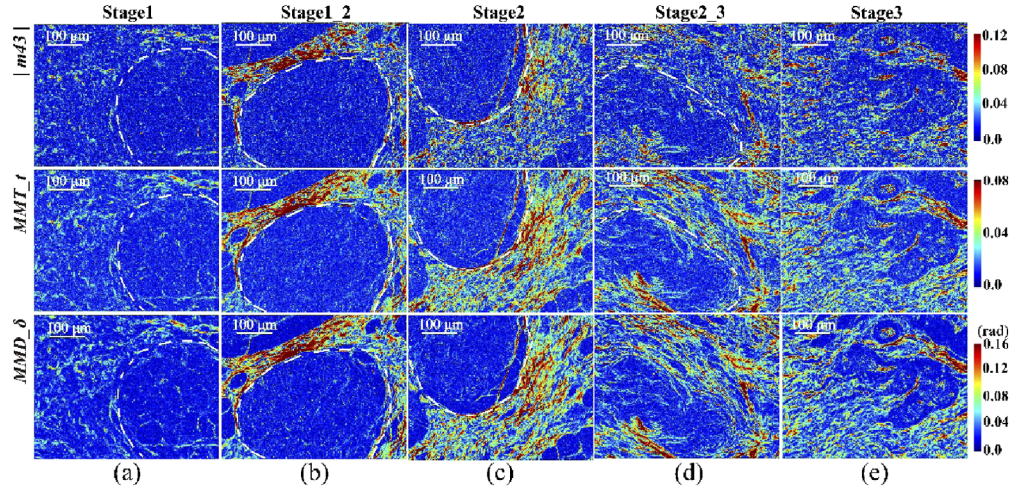


**Fig. 4.** Pseudo-color images of polarimetric parameters (the absolute value of Mueller matrix element |*m43*|, MMT parameter *t* and MMPD parameter *δ*) of the 12-μm-thick unstained dewaxed slices of breast duct tissue samples at different pathological stages: (a) stage 1 (normal); (b) stage 1_2 (between normal and ductal carcinoma *in situ*); (c) stage 2 (ductal carcinoma *in situ*); (d) stage 2_3 (between ductal carcinoma *in situ* and invasive ductal carcinoma); (e) stage 3 (invasive ductal carcinoma). The boundaries of the breast ducts are marked by the white dotted lines. The range of color bar is from 2th percentile to 98th percentile of each polarimetric parameter of all of breast ductal tissues at different pathological stages.

### 3.2. Quantitative characterization of polarimetric images of breast ductal carcinoma tissues at different stages

For quantitative analysis of the microstructural variations of breast ductal carcinoma tissues at different stages, in this section, the classification characteristic values-$f\_m, f\_std, f\_R, f\_u3, f\_U$ and $f\_e$-are calculated by using Eq. (S2) shown in Supplement 1 and presented in Table 1.

**Table 1. Six classification characteristic values for three Mueller matrix parameters.**

|  | $f\_m$ | $f\_std$ | $f\_R$ | $f\_u3$ | $f\_U$ | $f\_e$ |
|---|---|---|---|---|---|---|
| **\| *m43* \|** | 0.019 | 0.015 | 0.986 | 0.002 | 0.132 | 3.22 |
| ***t*** | 0.015 | 0.009 | 0.991 | 0.001 | 0.190 | 2.65 |
| ***δ*** | 0.028 | 0.017 | 0.983 | 0.003 | 0.113 | 3.49 |

Figure 5 illustrates the box plots of the statistical feature vectors $\overline{m}, \overline{std}, \overline{R}, \overline{u3}, \overline{U}$ and $\overline{e}$ extracted from |*m43*| of breast ductal carcinoma tissue samples from stage 1_2 to stage 3. Classification characteristic values (denoted by black or red solid lines for each statistical feature vector) and 378 components of statistical feature vectors (denoted as point clouds in different colors next to the corresponding box plots) are clearly displayed in this figure, from which we can obviously observe that the proportions of the components above and below the classification characteristic values represented by the solid lines are different in the process of carcinogenesis. The values of

scoring parameters ($N\_m$, $N\_std$, $N\_R$, $N\_u3$, $N\_U$ and $N\_e$) for breast ductal carcinoma tissue samples can be calculated by using Eq. (4) in Section 2.5.
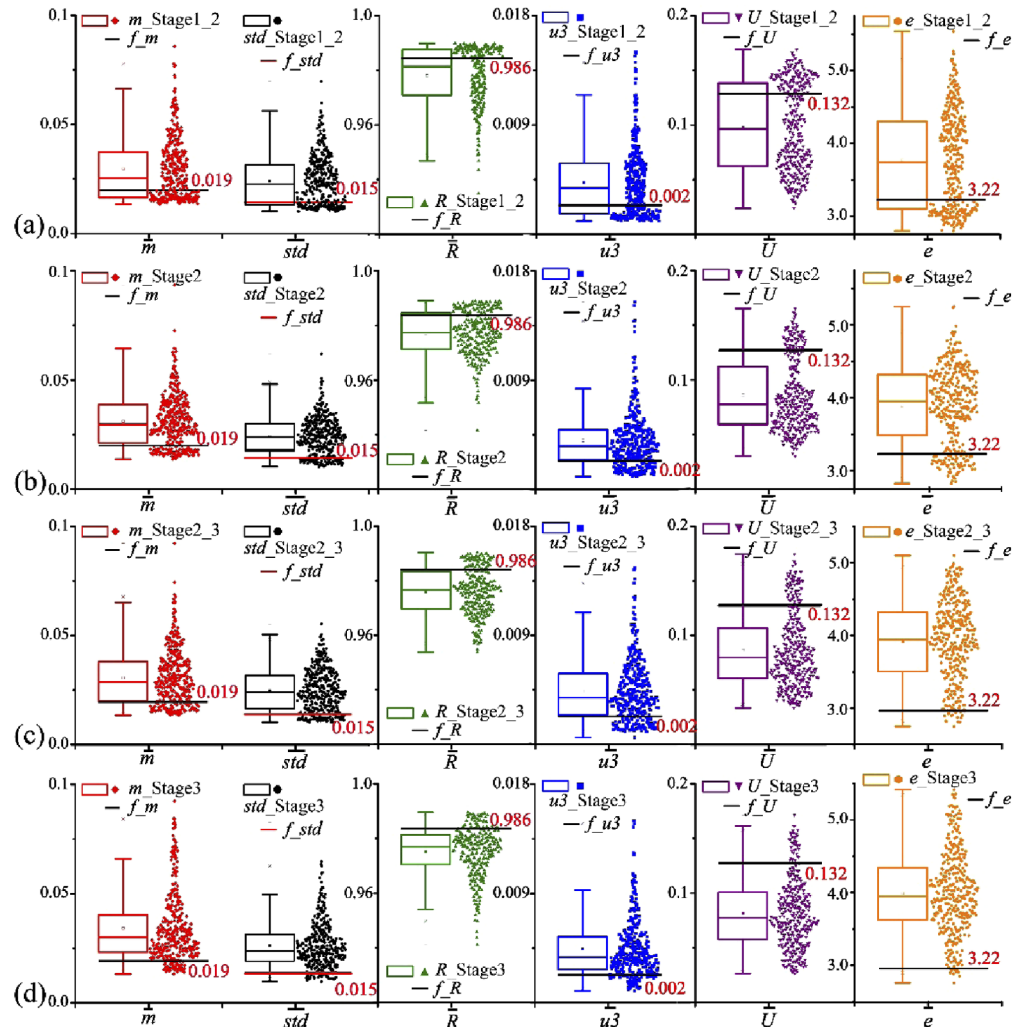


**Fig. 5.** Components of six statistical feature vectors extracted from $|m43|$ of breast ductal carcinoma tissue samples at different pathological stages: (a) stage 1_2; (b) stage 2; (c) stage 2_3; (d) stage 3. Classification characteristic values obtained from normal tissue samples are denoted by black or red solid lines for each statistical feature vector. 378 components of statistical feature vectors are denoted as point clouds in different colors next to the corresponding box plots.

*N_parameters* is sensitive to subtle change in distribution of FDHs of polarimetric parameters, to better distinguish among different stages of the breast ductal carcinoma tissues. Of note, random noise and outliers contribute little for the classification ability of *N_parameters* since: (1) although random noise would systematically shift the distribution of FDHs towards the right, all of our experiments were conducted under the same optical system, and it is reasonable to assume that they are subjected to the same distribution of noise. The FDHs of polarimetric parameters of all breast ductal tissues at different pathological stages would be subjected to the same systematic shift, which means the proposed method remains valid under random noise; (2)

The retardance related parameters are very sensitive to the fibrous structures and have strong specificity. Therefore, an outlier is rarely observed under normal experiment conditions. Besides, due to the fact that the polarimetic parameter image is divided into blocks for analysis, the effect of outliers is further reduced.

As indicated in Fig. 6(a), the values of *N_parameters* for Mueller matrix element |*m43*| of the samples shown in Fig. 5 change regularly with the pathological development of breast ductal carcinoma: (1) the values of *N_m*, *N_std*, *N_u3* and *N_e* increase significantly as the formation and metastasis of carcinoma cells from stage 1 to stage 3; (2) the values of *N_R* and *N_U* decrease monotonically in occurrence and progress of the lesion, and would approach 0 when carcinoma cells infiltrate the mammary tissue completely. Moreover, the values of *N_parameters* for corresponding MMT parameter *t* and MMPD parameter *δ* of these samples are also calculated and displayed in Figs. 6(b) and 6(c) respectively, which have the similar trends during the development processes from stage 1 to stage 3.
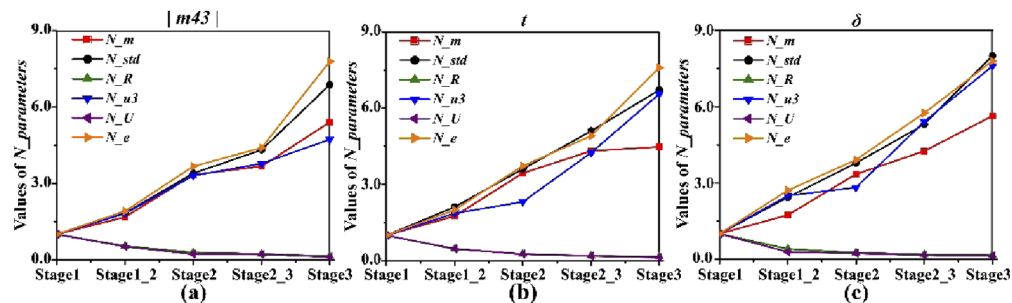


**Fig. 6.** Values of *N_parameters* of one sample in each pathological stage (from stage 1 to stage 3) for three polarimetric parameters: (a) absolute value of Mueller matrix element |*m43*|; (b) MMT parameter *t*; (c) MMPD parameter *δ*. The values of *N_parameters* in stage 1 are set as 1 used as criteria for evaluating other stages.

For a better confirmation of the observation above, the box plots of *N_parameters* of 10 samples in each pathological stage (from stage 1 to stage 3) for three Mueller matrix parameters are displayed in Fig. 7. We can clearly observe that for the three polarimetric parameters, the variation trends of all the *N_parameters* are monotonous and identical: (1) the *N_m* (red dots), *N_std* (black dots), *N_u3* (blue dots) and *N_e* (orange dots) values of all breast ductal carcinoma samples present obvious increasing trends during the development of breast ductal carcinoma, reaching the maximum 12.05 and minimum 3.07 in stage 3 from 1 in stage 1; (2) the values of *N_R* (green dots) and *N_U* (purple dots) for all samples show quick drops during carcinogenesis process, declining from 1 in stage 1 to the maximum 0.317 and minimum 0.041 in stage 3. When ductal carcinoma cells adequately invade surrounding tissues, they are supposed to approach the value of 0. On the other hand, Fig. 7 shows that the three Mueller matrix parameters have different abilities to distinguish different pathological stages of breast ductal carcinoma tissues based on the method of statistical feature vectors. Specifically, *N_parameters* of MMPD parameter *δ* have better contrasts than the other two parameters in differentiating samples in stage 2_3 from those in stage 2. However, compared with the |*m43*| and MMPD parameter *δ*, MMT parameter *t* is more powerful for characterizing samples in stage 3. It can be concluded from the above analysis that polarimetric parameters and their corresponding statistical feature vectors have potential to become quantitative indicators that can help determine the stage of the breast ductal carcinoma tissues.
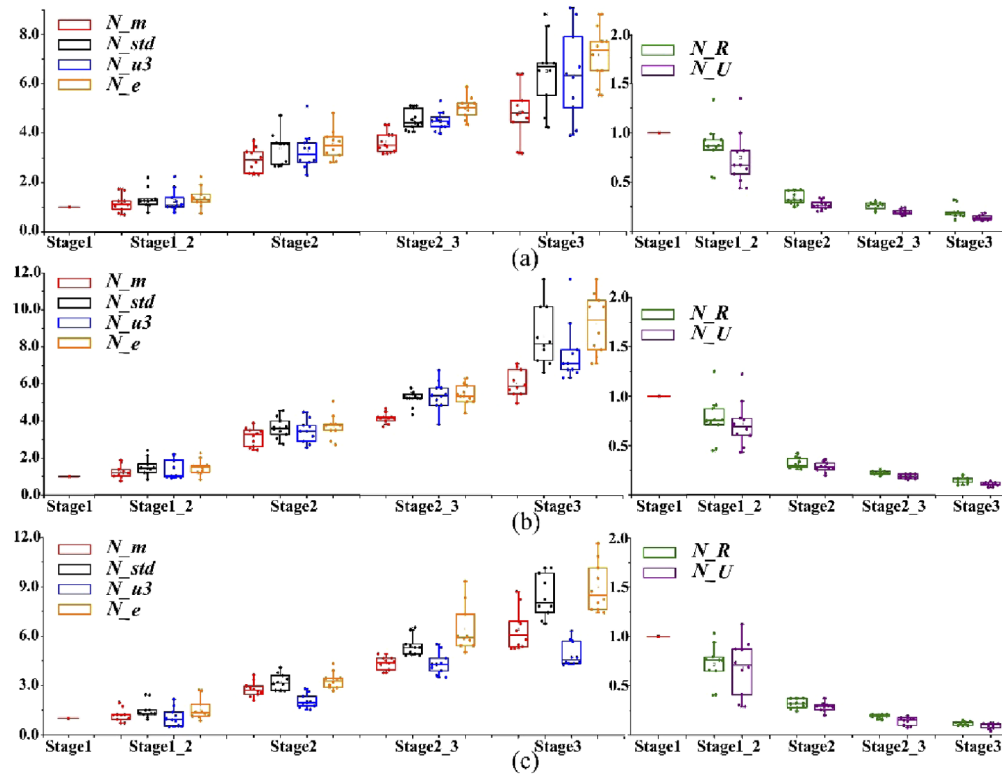
**Fig. 7.** Box plots of *N_parameters* of 10 samples in each pathological stage (from stage 1 to stage 3) for three polarimetric parameters: (a) absolute value of Mueller matrix element |*m43*|; (b) MMT parameter *t*; (c) MMPD parameter *δ*. The values of *N_parameters* in stage 1 are set as 1 used as criteria for evaluating other stages.

### 3.3.   Comparisons of characterization ability of different Mueller matrix parameters

For quantitative comparisons of differentiation ability of different Mueller matrix parameters for breast ductal carcinoma samples using statistical feature vectors, *r_values* of all experiments are calculated according to Eq. (5) in Section 2.6 and shown in Table 2. It can be observed from Table 2 that even though the absolute value of |*m43*| has excellent differentiation ability for breast ductal carcinoma samples in stage 2 and stage 1_2, its classification ability is generally worse than the other two parameters considering all stages. Compared with the *N_parameters* extracted from MMPD parameter *δ*, the values for MMT parameter *t* are better at differentiating breast ductal carcinoma samples in stage 2 from those in stage 1_2 and classifying samples in stage 3. In contrast, MMPD parameter *δ* has a better ability to make decision for samples between stages 1 and 1_2, as well as those between stages 2 and 2_3. Although both the MMPD and MMT parameters have the good ability in characterizing microstructures of breast ductal carcinoma tissues at different pathological stages, the calculation of MMT parameters is much faster than the MMPD parameters (0.004 s versus 57.18s for a Mueller matrix) under the same hardware condition (Intel(R) Core(TM)i7-9700 CPU and MATLAB 2019).

   Although further systematic analyses should be carried out, the preliminary results in this work demonstrate that the method of digitizing 2D Mueller matrix images into statistical feature vectors has the potential to facilitate characterizing the microstructural variations during the development of breast ductal carcinoma tissues quantitatively, resulting in the basis of automation of staging process and acceleration of diagnosis. Moreover, three Mueller matrix parameters

**Table 2. Values of r_values for all samples in two adjacent stages during carcinogenesis process.**

|  | N_m | N_std | N_R | N_u3 | N_U | N_e |
|---|---|---|---|---|---|---|
| **\| *m43* \|** | | | | | | |
| **Stage1- Stage1_2** | 0.402 | 0.173 | 0.729 | 0.169 | 0.618 | 0.197 |
| **Stage1_2- Stage2** | 0.000 | 0.000 | 0.000 | 0.000 | 0.000 | 0.000 |
| **Stage2- Stage2_3** | 0.284 | 0.283 | 0.263 | 0.376 | 0.196 | 0.161 |
| **Stage2_3- Stage3** | 0.404 | 0.163 | 0.637 | 0.149 | 0.223 | 0.107 |
| ***t*** | | | | | | |
| **Stage1- Stage1_2** | 0.289 | 0.105 | 0.453 | 0.076 | 0.393 | 0.138 |
| **Stage1_2- Stage2** | 0.000 | 0.000 | 0.000 | 0.000 | 0.000 | 0.000 |
| **Stage2- Stage2_3** | 0.025 | 0.024 | 0.000 | 0.678 | 0.075 | 0.137 |
| **Stage2_3- Stage3** | 0.000 | 0.000 | 0.072 | 0.057 | 0.000 | 0.000 |
| ***δ*** | | | | | | |
| **Stage1- Stage1_2** | 0.281 | 0.028 | 0.054 | 0.410 | 0.174 | 0.063 |
| **Stage1_2- Stage2** | 0.000 | 0.000 | 0.000 | 0.271 | 0.086 | 0.021 |
| **Stage2- Stage2_3** | 0.000 | 0.000 | 0.000 | 0.000 | 0.000 | 0.000 |
| **Stage2_3- Stage3** | 0.000 | 0.000 | 0.000 | 0.383 | 0.340 | 0.228 |

have been compared to show different evaluation abilities for different stages of breast ductal carcinoma tissue samples: (1) considering all the values of *N_parameters*, the MMT parameter *t* and MMPD parameter $\delta$ have good differentiation ability, and both of them are superior to the $|m43|$; (2) from the values of *N_m*, *N_std* and *N_R*, we can see that the MMPD parameter $\delta$ has more advantages than the other two parameters. The values of *N_parameters* between any two adjacent stages are close to or equal to 0 for the MMPD parameter $\delta$, indicating that this technique has a good application prospect in the field of quantitative staging of breast ductal carcinoma tissues.

## 4. Conclusion

In summary, we measured microscopic Mueller matrix images of breast ductal carcinoma tissues at different stages. The 2D images of Mueller matrix element $|m43|$, MMT parameter *t* and MMPD parameter $\delta$ of unstained breast duct tissue slices at different pathological stages were calculated and analyzed. For quantitative characterization, each Mueller matrix image was successively and evenly divided into 378 blocks from which six 378-dimensional statistical feature vectors can be obtained. After being evaluated by the corresponding classification characteristic value calculated from the statistical features of healthy duct tissue samples, 378 components in each statistical feature vector can be divided into two groups. Then a scoring parameter *N_parameters* was proposed based on the number of components in the two groups. We can conclude from the values of *N_parameters* of the statistical feature vectors for all of breast ductal carcinoma tissue samples at different stages that, the *N_m*, *N_std*, *N_u3* and *N_e* values experience a rapid rise with tumor initiation and progression, while the *N_R* and *N_U* present a quick drop during carcinogenesis process. Moreover, a comparative study showed that: the MMT parameter *t* and MMPD parameter $\delta$ have better characterization ability than the $|m43|$. The experimental results indicated that the microscopic Mueller matrix parameters combined with image processing method may have potential to provide monitoring indicators for quantitatively characterizing the microstructural variations of the breast duct tissues with carcinoma initiation and progress.

## Funding

## Disclosures

The authors declare no conflicts of interest.

See Supplement 1 for supporting content.

## References

1. O. Ginsburg, F. Bray, M. P. Coleman, V. Vanderpuye, A. Eniu, S. R. Kotha, M. Sarker, T. T. Huong, C. Allemani, A. Dvaladze, J. Gralow, K. Yeates, C. Taylor, N. Oomman, S. Krishnan, R. Sullivan, D. Kombe, M. M. Blas, G. Parham, N. Kassami, and L. Conteh, "The global burden of women's cancers: a grand challenge in global health," Lancet **389**(10071), 847–860 (2017).
2. D. M. Parkin, F. Bray, J. Ferlay, and P. Pisani, "Estimating the world cancer burden: Globocan 2000," Int. J. Cancer **94**(2), 153–156 (2001).
3. R. Siegel, K. Miller, and A. Jemal, "Cancer statistics 2019," Ca-Cancer J. Clin. **69**(1), 7–34 (2019).
4. A. Jemal, E. Ward, and M. J. Thun, "Recent trends in breast cancer incidence rates by age and tumor characteristics among U.S. Women," Breast Cancer Res. **9**(3), R28 (2007).
5. C. Brisken, K. Hess, and R. Jeitziner, "Progesterone and overlooked endocrine pathways in breast cancer pathogenesis," Endocrinology **156**(10), 3442–3450 (2015).
6. S. R. Lakhani, I. O. Ellis, S. J. Schnitt, P. H. Tan, and M. J. van de Vijver, "Invasive breast carcinoma," in *World Health Organisation classification of tumors of the breast*, F. Tavassoli and P. Devilee, eds. (Lyon, France, 2012).
7. National Comprehensive Cancer Network, "Breast cancer Clinical Practice Guidelines in Oncology," J. Natl. Compr. Cancer Network **1**(2), 148 (2003).
8. G. M. Nagaraja, M. Othman, B. P. Fox, R. Alsaber, C. M. Pellegrino, Y. Zeng, R. Khanna, P. Tamburini, A. Swaroop, and R. P. Kandpal, "Gene expression signatures and biomarkers of noninvasive and invasive breast cancer cells: comprehensive profiles by representational difference analysis, microarrays and proteomics," Oncogene **25**(16), 2328–2338 (2006).
9. R. Millikan, L. Dressler, J. Geradts, and M. Graham, "The need for epidemiologic studies of in situ carcinoma of the breast," Breast Cancer Res. Treat. **35**(1), 65–77 (1995).
10. L. Fulford, D. Easton, J. Reis-Filho, A. Sofronis, C. Gillett, S. Lakhani, and A. Hanby, "Specific morphological features predictive for the basal phenotype in grade 3 invasive ductal carcinoma of breast," Histopathology **49**(1), 22–34 (2006).
11. A. Elasbal, "Histochemical Patterns of Collagenic Fibers in the Benign and Malignant Breast Lesions," Adv. Breast Cancer Res. **08**(01), 1–10 (2019).
12. B. Saikia, K. Gupta, and U. N. Saikia, "The modern histopathologist: in the changing face of time," Diagn. Pathol. **3**(1), 25–29 (2008).
13. D. B. Strader, T. Wright, D. L. Thomas, and L. B. Seeff, "Diagnosis, management, and treatment of hepatitis C," Hepatology **39**(4), 1147–1171 (2004).
14. A. Golaraei, L. Kontenis, R. Cisek, D. Tokarz, S. J. Done, B. C. Wilson, and V. Barzda, "Changes of collagen ultrastructure in breast cancer tissue determined by second-harmonic generation double Stokes-Mueller polarimetric microscopy," Biomed. Opt. Express **7**(10), 4054–4068 (2016).
15. Y. Dong, J. Qi, H. He, C. He, S. Liu, J. Wu, D. S. Elson, and H. Ma, "Quantitatively characterizing the microstructural features of breast ductal carcinoma tissues in different progression stages by Mueller matrix microscope," Biomed. Opt. Express **8**(8), 3643–3656 (2017).
16. K. Burke, P. Tang, and E. Brown, "Second harmonic generation reveals matrix alterations during breast tumor progression," J. Biomed. Opt. **18**(3), 031106 (2012).
17. N. Ghosh and I. A. Vitkin, "Tissue polarimetry: concepts, challenges, applications, and outlook," J. Biomed. Opt. **16**(11), 110801 (2011).
18. V. V. Tuchin, "Polarized light interaction with tissues," J. Biomed. Opt. **21**(7), 071114 (2016).
19. H. He, R. Liao, N. Zeng, P. Li, Z. Chen, X. Liu, and H. Ma, "Mueller matrix polarimetry—an emerging new tool for characterizing the microstructural feature of complex biological specimen," J. Lightwave Technol. **37**(11), 2534–2548 (2019).
20. N. T. Clancy, S. Arya, J. Qi, D. Stoyanov, G. B. Hanna, and D. S. Elson, "Polarised stereo endoscope and narrowband detection for minimal access surgery," Biomed. Opt. Express **5**(12), 4108–4117 (2014).

21. Y. Dong, H. He, W. Sheng, J. Wu, and H. Ma, "A quantitative and non-contact technique to characterise microstructural variations of skin tissues during photo-damaging process based on Mueller matrix polarimetry," Sci. Rep. **7**(1), 14702 (2017).
22. Y. Dong, H. He, C. He, J. Zhou, N. Zeng, and H. Ma, "Characterizing the effects of washing by different detergents on the microstructures of silk fibers using Mueller matrix polarimetry," Int. J. Mol. Sci. **17**(8), 1301 (2016).
23. S. Liu, W. Du, X. Chen, H. Jiang, and C. Zhang, "Mueller matrix imaging ellipsometry for nanostructure metrology," Opt. Express **23**(13), 17316–17329 (2015).
24. C. He, H. He, J. Chang, Y. Dong, S. Liu, N. Zeng, Y. He, and H. Ma, "Characterizing microstructures of cancerous tissues using multispectral transformed Mueller matrix polarization parameters," Biomed. Opt. Express **6**(8), 2934–2945 (2015).
25. Y. Wang, H. He, J. Chang, C. He, S. Liu, M. Li, N. Zeng, J. Wu, and H. Ma, "Mueller matrix microscope: a quantitative tool to facilitate detections and fibrosis scorings of liver cirrhosis and cancer tissues," J. Biomed. Opt. **21**(7), 071112 (2016).
26. T. Liu, M. Lu, B. Chen, Q. Zhong, J. Li, H. He, H. Mao, and H. Ma, "Distinguishing structural features between Crohn's disease and gastrointestinal luminal tuberculosis using Mueller matrix derived parameters," J. Biophotonics **12**(12), e201900151 (2019).
27. C. He, J. Chang, Q. Hu, J. Wang, J. Antonello, H. He, S. Liu, J. Lin, D. S. Elson, P. Xi, H. Ma, and M. J. Booth, "Complex vectorial optics through gradient index lens cascades," Nat. Commun. **10**(1), 4264 (2019).
28. T. Liu, T. Sun, H. He, S. Liu, Y. Dong, J. Wu, and H. Ma, "Comparative study of the imaging contrasts of Mueller matrix derived parameters between transmission and backscattering polarimetry," Biomed. Opt. Express **9**(9), 4413–4428 (2018).
29. D. H. Goldstein, "Mueller matrix dual-rotating retarder polarimeter," Appl. Opt. **31**(31), 6676–6683 (1992).
30. J. Zhou, H. He, Z. Chen, Y. Wang, and H. Ma, "Modules design multiwavelength polarization microscope for transmission Mueller matrix imaging," J. Biomed. Opt. **23**(1), 016007 (2018).
31. R. M. A. Azzam, "Photopolarimetric measurement of the Mueller matrix by Fourier analysis of a single detected signal," Opt. Lett. **2**(6), 148–150 (1978).
32. S. Y. Lu and R. A. Chipman, "Interpretation of Mueller matrices based on polar decomposition," J. Opt. Soc. Am. A **13**(5), 1106–1113 (1996).
33. E. Du, H. He, N. Zeng, M. Sun, Y. Guo, J. Wu, S. Liu, and H. Ma, "Mueller matrix polarimetry for differentiating characteristic features of cancerous tissues," J. Biomed. Opt. **19**(7), 076013 (2014).
34. A. Pierangelo, S. Manhas, A. Benali, C. Fallet, J. Totobenazara, M. Antonelli, T. Novikova, B. Gayet, A. D. Martino, and P. Validire, "Multispectral Mueller polarimetric imaging detecting residual cancer and cancer regression after neoadjuvant treatment for colorectal carcinomas," J. Biomed. Opt. **18**(4), 046014 (2013).
35. N. Ghosh, M. F. Wood, and I. A. Vitkin, "Mueller matrix decomposition for extraction of individual polarization parameters from complex turbid media exhibiting multiple scattering, optical activity, and linear birefringence," J. Biomed. Opt. **13**(4), 044036 (2008).
36. H. He, J. Chang, C. He, and H. Ma, "Transformation of full 4×4 Mueller matrices: a quantitative technique for biomedical diagnosis," Proc. SPIE **9707**, 97070K (2016).
37. M. Sun, H. He, N. Zeng, E. Du, Y. Guo, C. Peng, Y. He, and H. Ma, "Probing microstructural information of anisotropic scattering media using rotation-independent polarization parameters," Appl. Opt. **53**(14), 2949–2955 (2014).
38. P. Li, D. Lv, H. He, and H. Ma, "Separating azimuthal orientation dependence in polarization measurements of anisotropic media," Opt. Express **26**(4), 3791–3800 (2018).
39. C. He, H. He, X. Li, J. Chang, Y. Wang, S. Liu, N. Zeng, Y. He, and H. Ma, "Quantitatively differentiating microstructures of tissues by frequency distributions of Mueller matrix images," J. Biomed. Opt. **20**(10), 105009 (2015).
40. V. A. Ushenko, O. V. Dubolazov, and A. O. Karachevtsev, "Two wavelength Mueller matrix reconstruction of blood plasma films polycrystalline structure in diagnostics of breast cancer," Appl. Opt. **53**(10), B128–B139 (2014).
41. M. Zaffar and A. Pradhan, "Assessment of anisotropy of collagen structures through spatial frequencies of Mueller matrix images for cervical pre-cancer detection," Appl. Opt. **59**(4), 1237–1248 (2020).
42. J. Chue-Sang, N. Holness, M. Gonzalez, J. Greaves, I. Saytashev, S. Stoff, A. Gandjbakhche, V. Chernomordik, G. Burkett, and J. Ramella-Roman, "Use of Mueller matrix colposcopy in the characterization of cervical collagen anisotropy," J. Biomed. Opt. **23**(12), 1 (2018).
43. H. F. Inman and E. L. Bradley, "The overlapping coefficient as a measure of agreement between probability distributions and point estimation of the overlap of two normal densities," Commun. Statist. –Theory Meth. **18**(10), 3851–3874 (1989).
44. R. C. Thomas and T. E. Janine, "Remodeling and homeostasis of the extracellular matrix: implications for fibrotic diseases and cancer," Dis. Models Mech. **4**(2), 165–178 (2011).
45. L. Kass, J. T. Erler, M. Dembo, and V. M. Weaver, "Mammary epithelial cell: influence of extracellular matrix composition and organization during development and tumorigenesis," Int. J. Biochem. Cell Biol. **39**(11), 1987–1994 (2007).

46. K. R. Levental, H. Yu, L. Kass, J. N. Lakins, M. Egeblad, J. T. Erler, S. T. Fong, K. Csiszar, A. Giaccia, W. Weninger, M. Yamauchi, D. L. Gasser, and V. M. Weaver, "Matrix crosslinking forces tumor progression by enhancing integrin signaling," Cell **139**(5), 891–906 (2009).

47. J. T. Erler and A. J. Giaccia, "The cellular microenvironment and metastases," in *Abeloff's Clinical Oncology*, M. D. Abeloff, J. O. Armitage, J. E. Niederhuber, M. B. Kastan, and W. G. McKenna, eds. (Churchill Livingstone, U.S., 2008).